The Meteoritical Society

Meteoritics & Planetary Science 1–18 (2016)
doi: 10.1111/maps.12612

Ni/S/Cl systematics and the origin of impact-melt glasses in Martian meteorite Elephant Moraine 79001

Christian M. SCHRADER[1,2], Barbara A. COHEN[1*], John J. DONOVAN[3], and Edward P. VICENZI[4]

[1]Marshall Space Flight Center, NASA, Huntsville, Alabama 35812, USA
[2]Geology Department, Bowdoin College, Brunswick, Maine 04011, USA
[3]Department of Chemistry, University of Oregon, Eugene, Oregon 97403, USA
[4]Smithsonian Institution, Museum Conservation Institute, Suitland, Maryland 20746, USA
[*]Corresponding author. E-mail: barbara.a.cohen@nasa.gov

(Received 01 December 2014; revision accepted 09 December 2015)

Abstract–Martian meteorite Elephant Moraine A79001 (EET 79001) has received considerable attention for the unusual composition of its shock melt glass, particularly its enrichment in sulfur relative to the host shergottite. It has been hypothesized that Martian regolith was incorporated into the melt or, conversely, that the S-enrichment stems from preferential melting of sulfide minerals in the host rock during shock. We present results from an electron microprobe study of EET 79001 including robust measurements of major and trace elements in the shock melt glass (S, Cl, Ni, Co, V, and Sc) and minerals in the host rock (Ni, Co, and V). We find that both S and major element abundances can be reconciled with previous hypotheses of regolith incorporation and/or excess sulfide melt. However, trace element characteristics of the shock melt glass, particularly Ni and Cl abundances relative to S, cannot be explained either by the incorporation of regolith or sulfide minerals. We therefore propose an alternative hypothesis whereby, prior to shock melting, portions of EET 79001 experienced acid-sulfate leaching of the mesostasis, possibly groundmass feldspar, and olivine, producing Al-sulfates that were later incorporated into the shock melt, which then quenched to glass. Such activity in the Martian near-surface is supported by observations from the Mars Exploration Rovers and laboratory experiments. Our preimpact alteration model, accompanied by the preferential survival of olivine and excess melting of feldspar during impact, explains the measured trace element abundances better than either the regolith incorporation or excess sulfide melting hypothesis does.

INTRODUCTION

Martian meteorite Elephant Moraine A79001 (EET 79001) comprises two crystalline igneous lithologies and pods and veins of glassy material. Of the crystalline portions, Lithology A (Lith A), an olivine-phyric shergottite, has a basaltic groundmass hosting megacrysts and clusters of olivine, pyroxene, and chromite (McSween and Jarosewich 1983; Goodrich 2002); the megacrystal population was termed "lithology X" by Treiman (1995) under the assumption that it was xenocrystic. In linear contact with Lith A is Lithology B (Lith B), a basaltic shergottite (McSween and Jarosewich 1983). Shock effects evident in EET 79001 include mosaicism, pervasive fracturing of igneous pyroxene and olivine, amorphization of plagioclase throughout the host rock, and formation of high-pressure minerals such as ringwoodite associated with extensive pockets of shock melt (e.g., Walton 2013).

Glass-dominated pockets and veins (Lithology C or Lith C) in EET 79001 likely formed by local shock effects concentrated in or along vugs connected by veins and fractures, and hereafter called shock melt (Mittlefehldt et al. 1999; Walton 2013). Lith C is locally drusy with quench crystals (crystallites), entrained megacrysts, and vesicles (McSween and Jarosewich 1983). Gooding and Muenow (1986) reported aluminosilicates and Gooding et al. (1988) reported carbonate and sulfate phases in Lith C that they interpreted to be from regolith incorporation, in situ

weathering, or hydrothermal alteration. The multiple lithologies and the abundant shock melt glass make EET 79001 unique among achondrites and it has been correspondingly well studied.

Most of EET 79001's Lith C is hosted in Lith A. McSween and Jarosewich (1983) interpreted Lith C to approximate the bulk composition of Lith A but with excess incorporation of melted plagioclase. Rao et al. (1999) showed that Lith C glass is enriched in S as well as the feldspar components Al, Ca, and Na, and depleted in Mg and Fe relative to Lith A; they suggested that a Martian regolith (referred to as "soil") component was incorporated into the melt along with excess plagioclase. Rao et al. (2003, 2004, 2008) expanded their investigation of EET 79001 and extended their Martian regolith hypothesis to Zagami and Shergotty, in which the shock melt has similar enrichments and depletions relative to the host rocks as EET 79001. The Tissint shergottite, recovered as a fresh fall in 2012, shows many similarities to lithologies A and C of EET 79001, including a similar cosmic-ray exposure age (Aoudjehane et al. 2012). Refractory trace element, sulfur, and fluorine data for the matrix and glass veins in Tissint have been argued to result from incorporation of Martian surficial weathering products (Aoudjehane et al. 2012).

Because we have no known samples of regolith from Mars available for study, the possibility of extracting compositional information regarding Martian regolith from meteoritic samples is attractive. The mineralogy, chemistry, and isotopic composition of Martian regolith can illuminate past and ongoing processes on the surface and near-surface of the planet, such as impact gardening, volcanism, and hydrothermal activity (Newsom and Hagerty 1997; Newsom et al. 1999; Bishop et al. 2002; Rao et al. 2002, 2009). Therefore, it is important to understand whether the composition of Lith C can be explained by incorporation of Martian regolith. Walton et al. (2010) proposed that no Martian regolith component is necessary to explain the excess S in the pods of EET 79001 shock melt they investigated, instead suggesting preferential melting of Lith A sulfides. It is probable that the glassy lithology in both meteorites is highly heterogeneous, as Barrat et al. (2014) investigated glass pockets in both Tissint and EET 79001 using high precision LA-ICP-MS and found no trace element signatures that would implicate a Martian surface contribution. Nonetheless, it is clear that the portions of the shock glass in both meteorites have elemental characteristics different from the host lithology that are worthy of further investigation. Here, we use new analyses of several glassy areas within EETA 79001 shock melt, along with improved compositional data for surface rocks and regoliths from the Mars Exploration Rover (MER) alpha particle X-ray spectrometer (APXS) (Gellert et al. 2004, 2006; Rieder et al. 2004; McSween et al. 2008), to provide tighter constraints on potential endmember components. While previous studies have addressed this using the major element and S compositions of Lith A and Lith C, we expand this inquiry using data for Ni, Co, V, Sc, and Cl.

Martian regolith is not homogeneous but current data demonstrate some useful consistencies. Along with S, Ni and Cl are significantly enriched in Martian regolith: Gusev and Meridiani basaltic regoliths together average 5.95 wt% SO_3, 467 ppm Ni, and 0.69 wt% Cl (Yen et al. 2006). Pathfinder and Viking regolith analyses are similarly high in SO_3 and Cl (Yen et al. 2005). Yen et al. (2005) discuss the presence of a global dust component ("bright dust") in all Martian regolith and intact rock surface compositions, and that this bright dust is approximately 50% enriched in Cl, SO_3, and Ni relative to MER-A and MER-B darker regolith compositions. However, even without the bright dust component, Martian regoliths analyzed in situ are elevated in Ni, S, and Cl relative to fresh rock surfaces, and this enrichment appears to be a global characteristic (Yen et al. 2005, 2006; Blake et al. 2013). In fact, elevated Ni, along with Ti and K, in the surface breccia meteorite NWA7034/7533 (Black Beauty), has been taken as an indication that this meteorite contains significant amounts of wind-blown dust (Humayun et al. 2013). We use an average of MER-A basaltic soil compositions (Yen et al. 2006) in our mixing models, which is similar to basaltic soils measured by other Mars missions (Yen et al. 2005; Blake et al. 2013).

If Martian regolith is indeed a contributor to Lith C's budget, both Ni and Cl should show elevated abundances, in addition to S. Similarly, the sulfide trace minerals in EET 79001, which are dominantly pyrrhotite (McSween and Jarosewich 1983), contain more Ni by concentration than any other phase in Lith A. Therefore, we use Ni abundance and Ni/S to assess the roles of regolith and/or excess sulfide in the shock melt, and Cl abundance to assess the role of regolith in Lith C. Additionally, we constrain the contribution of Lith A minerals to the shock melt using Co. We examined two samples of EET 79001 that include shock melt pockets and basaltic wallrock (Lith A). We find that either a regolith or an excess sulfide component, along with excess plagioclase and residual olivine, can explain most of the major element and S abundances in the shock melt. However, we show that trace element abundances, particularly Ni, preclude either sulfide or regolith as the source of the S under any simple mixing or fractionation model. Moreover, we find that incorporation of the common secondary minerals found

in cracks and vugs in EET 79001 satisfies major- and trace element constraints in the shock melt composition. We therefore propose a model by which the EET 79001 parent rock was exposed to either hydrothermal alteration or chemical weathering in a near-surface Martian environment prior to impact, but which does not include the incorporation of comminuted surface material.

METHODOLOGY

Samples

Two thin sections of Lithology A were investigated —EET 79001,18 and EET 79001,53. Both contain shock melt pockets of broadly basaltic composition hosted by Lith A. Figure 1 shows the petrographic relationships between basalt and the shock melt, entrained crystals, and vesicles. The shock melt contains entrained olivine grains, schlieren of feldspathic glass, and quench crystals of pyroxene and olivine (we identified mineralogy via a combination of optical microscopy and electron microprobe composition, so we cannot distinguish between low- and high-pressure polymorphs in this study). Figure 1a shows that EET 79001,53 contains vesicles that increase in size from one edge of the melt pocket to the other, indicating migration and coalescence of a vapor phase. EET 79001,53 also contains megacrystic olivine concentrated in the opposite end of the pocket from the largest vesicles. Figures 1b and 1e show that EET 79001,18 contains more crystal-free glass than does EET 79001,53. In EET 79001,53, crystal-free glass is restricted to the vesicle-free edges of the melt pocket and the melt veins (Fig. 1c), which quenched first. Both sections contain sulfides (pyrrhotite with minor pentlandite solid solution) in the shock melt as grains ranging from submicron- to ~5 micron-sized sulfide globules to subrounded larger grains (Fig. 1e). These textures represent a reaction of the original minerals with the melt, and the smallest globules likely represent an unmixing of a sulfide liquid from a sulfide-saturated melt before and during quenching.

We recognize four types of glasses in the shock melt. The majority of the glass is basaltic and here termed shock melt. Feldspathic glass (sensu lato) ranges from maskelynite in Lith A that maintains its crystal habit to diffuse schlieren in Lith C mixed with the basaltic shock melt (Fig. 1e). This was termed "clear glass" by McSween and Jarosewich (1983) to distinguish it from the basaltic "brown glass." In addition, we share the observation of other glass types with Walton et al. (2010): small pockets of glass with relatively high-Z (high average atomic number) corresponding to brighter colors in backscattered-electron (BSE) imaging, are basaltic areas with a larger contribution of pyroxene than typical shock melt; and, at the edges of the melt pockets are small irregular patches of P- and Ca-rich glass that we interpret to represent unmixed domains of melted Ca-phosphate. Here we are concerned with the basaltic shock melt glass. EET 79001,18 contains relatively large (10–100's μm) crystal-poor to crystal-free domains (Fig. 1b), which we analyzed by transect. The shock melt in EET 79001,53 is quench crystal- and vesicle-rich (Fig. 1a), but has a crystal-poor region 10–100 μm thick at the melt contact with Lith A, which we interpret to be the first quenched melt; we targeted this region for transects.

Electron Microprobe Analysis

For all quantitative analyses, we used the Cameca SX100 electron microprobe at the CAMCOR facility in Eugene, Oregon, running at 15 kV with a 5 μm beam size, except in a few instances where the size of the phase demanded a smaller beam size. Silicate, synthetic oxide, and metal standards were used for calibration. For all analyses, Phi-Rho-Z algorithms were used for matrix and interference corrections and standard intensities were corrected for beam current drift over time (Armstrong 1988; Donovan et al. 1993; Reed 2005).

For all analyses, and especially the glass analyses, we used time dependent intensity (TDI) corrections for loss (or gain) during analysis using a self-calibrated correction to account for volatilization of Na, K, and Si within the Probe for EPMA software (Donovan 2014). In general, corrections for loss (or gain) analytical artifacts, analysts reduce beam current, increase beam diameter, decrease beam exposure (acquisition) time, and/or cool the sample, along with a software correction for these effects which, depending on the element, can result in decreases or increases in X-ray intensity over time. The physics of ion migration/volatilization as a function of thermal conductivity, ion mobility, and electron dose is complex and very likely convolves together several different physical processes with different time scales. Therefore, the intensity change over time is more than a simple exponential. By fitting the log intensity to a quadratic and extrapolating again, one may improve the accuracy of the TDI correction considerably without having to reduce beam current or increase beam diameter, even for beam-sensitive phases such as hydrous glass (Donovan et al. 1993). For shock melt glass analyses, the range of corrections in relative % of counts per second was Na: −5 to +185% (most were +40 to 70%), K: −18 to +13%, and Si: −3 to +2%.

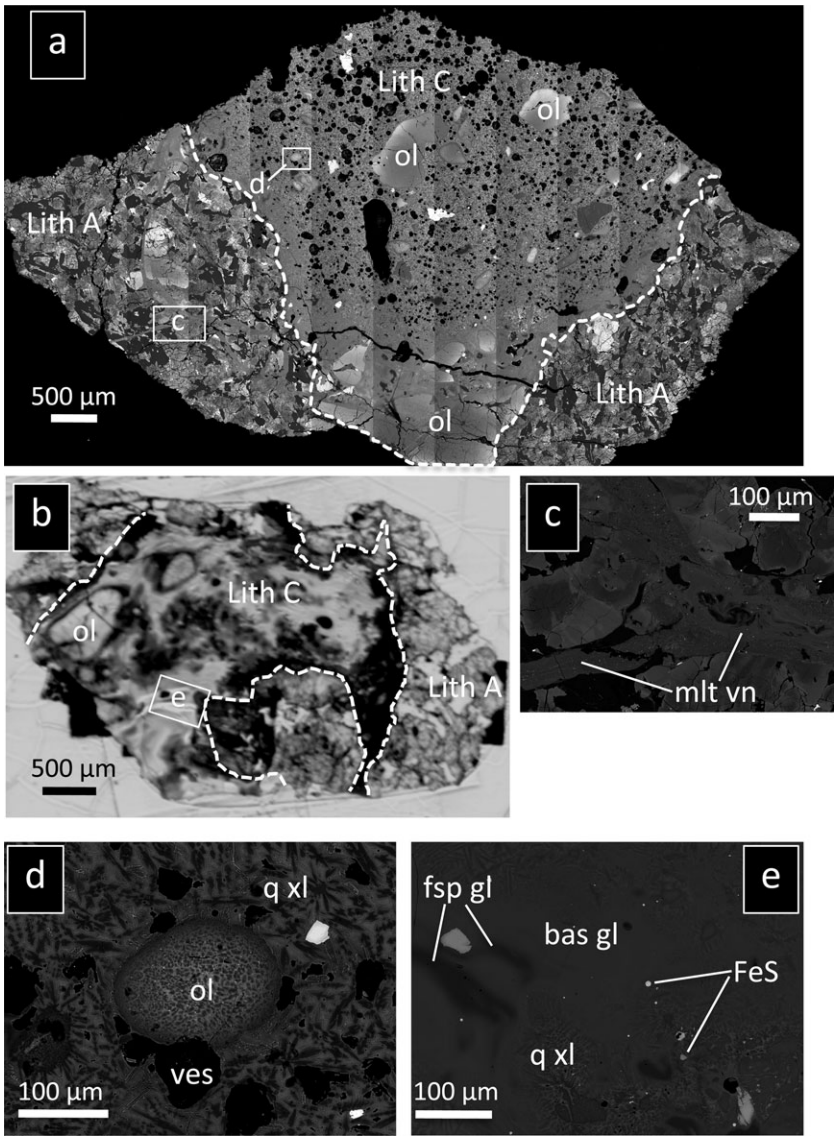

Fig. 1. Backscattered-electron and optical images of EET 79001,53 and EET 79001,18. a) Composite backscattered-electron image (BSI) of EET 79001,53. The dashed line delineates the border between the basaltic Lith A and the melt glass-dominated Lith C; boxes indicate the regions of image 1c and 1d; ol = olivine. b) Optical scan of thin section EET 79001,18 indicating the location of 1e. Dark areas of Lith C are quench crystal-dominated. Quench crystals nucleate on the walls of the melt pocket and on the entrained olivine grains. c) BSI of shock melt vein (mlt vn) feeding into the Lith C glass. d) Recrystallized olivine grain surrounded by quench crystals (q xl) and vesicles (ves). Most of the quench crystals are pyroxene but olivine crystals nucleate on the grain. e) Shock melt with schlieren of feldspathic glass (fsp gl) in basaltic glass (bas gl). Two populations of pyrrhotite (FeS) are indicated: a subrounded, primary, entrained grain, and globules of pyrrhotite that are either melted and remobilized or may represent unmixing from the sulfur-saturated shock melt.

For each olivine and pyroxene analysis, Na, Al, Mg, Ca, Ti, Fe, Mn, K, and Si were determined with a 30 nA current followed by Ti, Cr, Ni, Co, P, V, Zn, and Cu at 100 nA. Counting times were 40 to 120 s on peaks and 20 to 80 s off peaks. The 3σ detection limits were: 75–95 ppm for Ni and Co, 60–65 ppm for P_2O_5 and V, 100–115 ppm for Na_2O and K_2O, 135–140 ppm for Cr, and 35–40 ppm for Ti. We analyzed 3–6 points for each core and each rim of silicate minerals, and we analyzed transects across the shock melt (Fig. 1d).

Sulfides and Fe-Ti oxides were analyzed for Si, Mg, Ca, Fe, Mn, S, Ti, Cr, Ni, Co, V, Zn, Cu, and O with a 50 nA current. The 3σ detection limits were 130–250 ppm for Co, Ni, Zn, Cu, and Cr; 30–60 ppm for Ca, Mg, Mn, and Ti; and 100–200 ppm for O. Most

sulfide grains are unmixed and/or altered and these grains were analyzed by a cluster of points chosen to representatively cover all phases.

In glasses, Na, Al, Mg, Ca, Ti, Fe, Mn, K, Cr, Si, and S were determined with a 30 nA current followed by F, Sc, Ni, Co, P, V, Cl, and I at 100 nA. Counting times were 60 to 320 s on peaks and 20 to 320 s off peaks. These conditions may seem extreme for glass analysis, but have been shown to yield good results when coupled with the TDI technique for hydrous glasses. At the 99% (3σ) confidence level, detection limits (d.l.) were: 35–45 ppm for Ni, Co, and V; 10–13 ppm for Sc; and 50–55 ppm for Cl. Glasses were analyzed as transects across melt pockets and veins and in clusters on areas of interest.

We conducted wavescans on multiple spots in the shock melt glass and on anhydrite and pyrrhotite standards to assess the sulfur speciation in the glass after Wallace and Carmichael (1994). Additional semi-quantitative element maps and backscattered-electron images were obtained with the CAMCOR instrument and using the field emission JEOL JXA-8530F Hyperprobe at the SENCR-MIC facility in Fayetteville, North Carolina. A data table containing all of our shock melt analyses may be found in Appendix S1.

RESULTS

Phase Compositions and Occurrences

Table 1 shows our analyses of Lith A and Lith X silicates. Olivine and pyroxene grains entrained in the shock melt (Lith X) are subrounded with intact cores and are surrounded by quench crystals (Figs. 1a and 1b). Some smaller olivine grains in the shock melt are rounded and now composed of multiple equant, euhedral crystals with granular texture, suggesting they were melted during shock and recrystallized without disaggregating into the melt (Fig. 1d). Silicate mineral compositions within Lith A and Lith X are shown in Table 1. Lith X olivine cores from EET 79001,53 contain 470–570 ppm Ni and have Mg#'s (molar 100*Mg/Mg+Fe) of 72–75, while the rims have Mg#'s of 61–64 and Ni contents of 280–380 ppm. In all olivine analyses, Co is generally present from 80–115 ppm. All measured olivines contained less than the ~65 ppm detection limit of V. Pyroxenes contained less Ni and Co but measurable V.

Table 2 contains an average sulfide composition garnered from 18 analyses across both thin sections. Pyrrhotite in Lith A was a late crystallizing phase interstitial to olivine, pyroxene, and plagioclase feldspar. Pyrrhotite in the shock melt occurs in two modes, both shown in Fig. 1e: entrained subhedral primary sulfide grains with irregular edges that have reacted with the shock melt, and as small globules (<5 μm) that may represent unmixing from the sulfide-saturated shock melt (Walton et al. 2010). Most of the sulfide globules are too small for reliable analysis by WDS. The average in Table 2 is from spots with non-O totals of >98 wt%. Pyrrhotite grains are partly exsolved into higher- and lower-Ni domains, although the total range of Ni is narrow (0.5–2.6 wt%).

In this work, we consider the shock melt composition to be the average glass composition, exclusive of relic crystals. Table 3 compares shock melt compositions from our work and others', including Walton et al.'s (2010) calculated composition of a crystal-rich domain, to Lith A. Figure 2 shows the composition of the basaltic and feldspathic melts, Lith A silicates, and the Lith A whole rock composition of McSween and Jarosewich (1983). The basaltic shock melts cluster near the Lith A composition but lie along a mixing line with feldspathic glass and Lith A maskelynite compositions. Some of the basaltic shock melt compositions project toward more Mg-rich compositions than the Lith A olivine and others fall between Lith A and the Lith A pigeonite compositions, but none are as magnesian as the Lith A and olivine compositions. These data support the petrographic observation that Lith A olivine is underrepresented in the shock melt lithology, while feldspar is incorporated in excess relative to Lith A.

The shock melt glass we investigated is enriched in Al, Ca, Na, and S and depleted in Ti, Cr, Fe and Mg, relative to Lith A (Fig. 3), as noted first by Rao et al. (1999). Additionally, the shock melt is depleted in P and K. Walton et al. (2010) calculated the compositions of melt pockets by using modal analyses to apportion compositional attributes of quench crystals and interstitial melt, and found they approximated the composition of Lith A. We and Rao et al. (1999), on the other hand, find a dominantly basaltic melt composition by direct analysis of glassy areas far from quench crystals that is more dissimilar to Lith A and does not match Walton et al.'s (2010) integrated liquid composition. Undoubtedly, each shock melt pocket in EET 79001 is somewhat unique.

Figure 4 shows our trace element compositions of the shock melt normalized to Lith A and the Lith A groundmass composition values (Mittlefehldt et al. 1999; Warren et al. 1999). The shock melt contains a 65% excess of Sc relative to Lith A and 35% excess relative to its groundmass. Although we did not determine Sc contents for mineral phases, the major carrier of Sc in EET 79001 is pyroxene, and especially megacrystal

Table 1. EET 79001 bulk and mineral compositions.

	Bulk Lithology A[a]	Lithology A groundmass[b]	Lithology A maskelynite	Lithology A pyroxene	Lithology A olivine	Lithology A merrilite[c]	Lithology X olivine core[d]	Lithology X olivine core[d]	Lithology X olivine rim[d]	Lithology X pyroxene core[d]
wt%			average, $n = 9$	average, $n = 9$	average, $n = 9$			example	example	example
SiO_2	48.5	49.2	53.8	52.1	37.9	n.a.	37.6	37.2	40.0	50.5
TiO_2	0.70	0.78	0.05	0.27	0.08	n.a.	b.d.l.	0.07	0.08	0.56
Al_2O_3	5.68	6.44	29.2	0.85	0.19	0.01	b.d.l.	0.04	0.30	0.80
Cr_2O_3	0.58	0.12	0.02	0.30	0.08	n.a.	0.06	0.05	0.07	0.26
FeO	18.5	18.4	0.79	22.4	28.5	4.28	27.1	30.0	16.1	26.9
MnO	0.42	0.42	0.02	0.52	0.41	0.20	0.43	0.47	0.30	0.41
MgO	16.6	14.4	0.20	17.0	31.2	1.70	33.5	32.0	41.2	14.3
CaO	7.10	7.96	11.4	5.39	0.69	46.8	0.20	0.24	0.62	5.17
Na_2O	0.84	0.97	4.87	0.07	b.d.l.	0.67	b.d.l.	b.d.l.	b.d.l.	b.d.l.
K_2O	0.05	0.06	0.15	b.d.l.	b.d.l.	0.04	b.d.l.	0.02	0.13	0.07
P_2O_5	0.65	0.75	0.03	b.d.l.	0.03	46.9	0.02	b.d.l.	b.d.l.	n.d.
SO_3	0.45	0.52	0.02	b.d.l.	0.05	n.a.	b.d.l.	b.d.l.	b.d.l.	n.d.
ppm										
Ni	145	100	b.d.l.	202	471	n.a.	438	1061	1831	566
Co	49	42	28	214	324	n.a.	b.d.l.	b.d.l.	197	b.d.l.
Sc	38	45	16	n.d.	n.d.	n.a.	n.d.	n.d.	n.d.	n.d.
V	225	n.a.	51	b.d.l.	b.d.l.	n.a.	b.d.l.	b.d.l.	999	b.d.l.
Cl	26	n.a.	51	n.d.	n.d.	n.a.	n.d.	n.d.	n.d.	n.d.

[a]SiO_2 through SO_3 from McSween and Jarosewich (1983); Ni through V from Warren et al. (1999); Cl from Burghele et al. (1983).
[b]SiO_2 through SO_3 from McSween and Jarosewich (1983); Ni through Sc from Mittlefehldt et al. (1999).
[c]Steele and Smith (1982).
[d]Representative analysis.
n.d. = not detected; b.d.l. = below detection limit; n.a. = not analyzed.

Table 2. Average sulfide compositions (n = 18) in EETA79001,18 and 53 Lith A.

	Average (n = 18)	SD	Min	Max
wt%				
Si	0.03	0.02	b.d.l.	0.04
Mg	0.00	0.01	b.d.l.	0.02
Ca	0.05	0.02	0.02	0.11
Fe	60.5	1.94	58.1	65.3
Mn	0.05	0.03	0.01	0.13
Ti	0.11	0.17	b.d.l.	0.42
Cr	0.03	0.02	b.d.l.	0.08
Ni	1.11	0.64	0.52	2.57
Co	0.11	0.04	0.05	0.16
V	b.d.l.	0.01	b.d.l.	0.01
Zn	b.d.l.	0.03	b.d.l.	0.01
Cu	0.20	0.06	0.07	0.26
S	36.6	2.51	29.9	38.3
Total	98.8			

b.d.l. = below detection limit

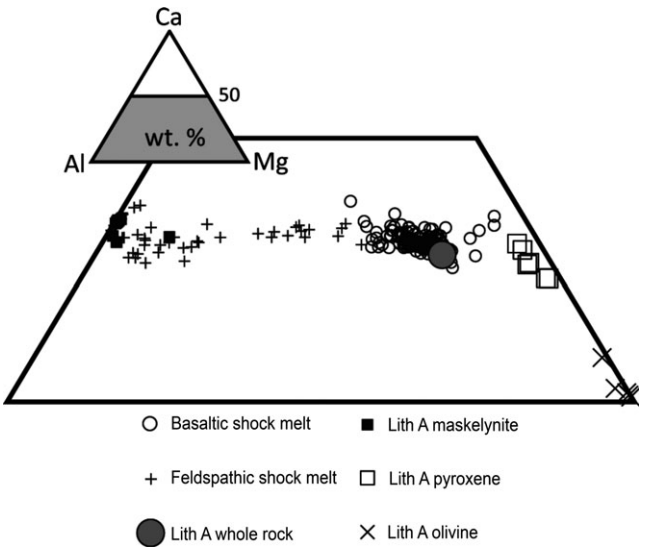

Fig. 2. Lith C and Lith A phases plotted with the Lith A whole rock composition in a portion of the Al-Ca-Mg ternary system. The values are in wt% and the quadrilateral extends to Ca_{50}.

pyroxene (Smith et al. 1984; Mittlefehldt et al. 1999). Mittlefehldt et al. (1999) interpreted their groundmass Sc contents to be high due to sampling error during microcoring, so our shock melt enrichment in Sc relative to the groundmass is a minimum estimate. Cobalt is appreciably enriched in the basaltic shock melt relative to both Lith A and its groundmass, but because olivine, pyroxene, and sulfide are all major carriers of Co in EET 79001 (Steele and Smith 1982; Lorand et al. 2005; Herd et al. 2009), the source is difficult to trace. These trace element normalizations show that some mafic component is incorporated into the shock melt beyond its proportion in the groundmass, and at least some of this mafic component is Lith A pigeonite.

Quantitative Mixing Relationships

The first-order observation of the element depletions and enrichments in Figs. 3 and 4 suggests that, in addition to S enrichment, the shock melt glass is enriched in some plagioclase components (Al, Ca, and Na, but not K) and depleted in components of mafic silicates and oxides and spinels (Mg, Fe, Ti, and Cr) and phosphate components (P).

Here, we address whether the shock melt composition could have been derived from Lith A with the addition of sulfide or Martian soil. We do this using least squares, mass balance calculations for major elements using the model of Korotev et al. (1995), the results of which are shown in Table 4. These models use as inputs the Lith A whole rock and major mineral compositions (Table 1), normalized to 100% and converted to element wt%, and mixes them to match our bulk Lith C composition (Table 3). The model weights each element by the uncertainty in the Lith C composition (elements with greater standard deviations are given less weight in the model), but treats the inputs without weighting. Given that the inputs incorporate the average composition taken from many sources, the representativity of the input compositions may be a factor, but the results shown below are not very sensitive to small variations in input composition and are intended to be only illustrative. The residuals of the weight % oxides in model integrated composition versus the Lith C composition are summed and squared to assess the fit. The value of $\chi 2/\nu$ (reduced chi-square) should approximate unity for a good fit. Values greater than unity represent poorer fits but values less than unity do not indicate significantly better fits.

Model 1 tests the Rao et al. (1999) hypothesis of added Martian regolith using an average of MER-A Martian basaltic regolith compositions from Yen et al. (2006). As discussed in the introduction, there is likely not a single global Martian regolith composition; however, average basaltic soil compositions from MER-A and MER-B are strikingly similar to each other and to Pathfinder and Viking analyses (Yen et al. 2005, 2006). Thus, the MER-A average composition is as good a proxy as we have for Martian regolith from unknown sites. Model 2 tests the Walton et al. (2010) hypothesis of preferential melting of sulfides by using our average pyrrhotite composition. The model results, relative to the Lith C composition, are shown in Fig. 5a. For both models, olivine is the restite (negative

Table 3. EET 79001 Lith C compositions and potential sources of sulfur used in mixing models.

	Lithology C, this study (n = 164)	1σ	Lithology C Walton et al. (2010)	Lithology C Rao et al. (1999)	Lithology A sulfide[a]	Gusev basaltic soil[b]
wt%						
SiO_2	50.0	0.68	51.1	49.5	0.04	46.3
TiO_2	0.52	0.06	0.36	0.52	0.11	10.1
Al_2O_3	6.33	1.18	14.1	7.26	n.a.	0.87
Cr_2O_3	0.48	0.04	0.26	0.48	0.03	0.35
FeO	17.2	0.73	11.9	17.1	45.5	16.0
MnO	0.39	0.02	0.34	0.45	0.04	0.32
MgO	14.8	0.98	9.56	14.8	b.d.l.	8.60
CaO	7.59	0.43	9.20	7.70	0.04	6.34
Na_2O	0.94	0.25	2.06	0.98	n.a.	3.00
K_2O	0.04	0.01	0.08	0.04	n.a.	0.44
P_2O_5	0.48	0.22	0.36	–	n.a.	0.82
SO_3	0.55	0.13	0.81	0.77	53.4	6.00
ppm						
Ni	100	33	–	–	8243	465
Co	59	18	–	–	1100	–
Sc	62	12	–	–	n.a.	–
V	201	41	–	–	n.a.	–
Cl	57	22	–	–	n.a.	7211

[a]Calcuated on an oxide renormalized basis from Table 2.
[b]Yen et al. (2006)
b.d.l. = below detection limit; n.a. = not analyzed; – not reported.

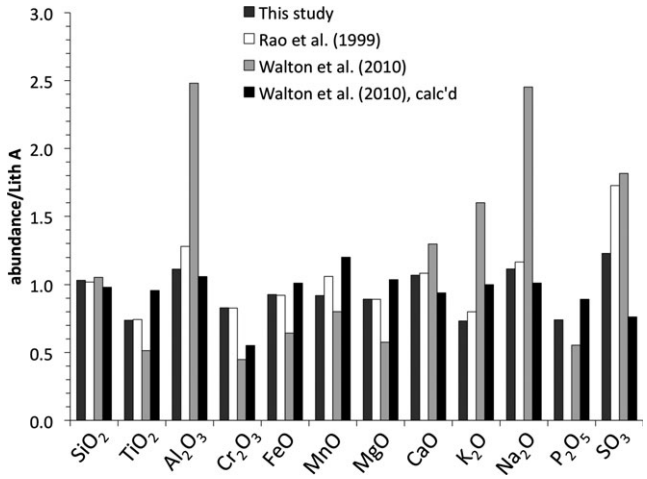

Fig. 3. Basaltic shock melt glass compositions from this study (n = 164), Rao et al. (1999), and Walton et al. (2010) normalized to the Lith A whole rock composition of McSween and Jarosewich (1983). All compositions are shown in Table 3. The Walton et al. (2010) "calc'd" composition was integrated from a grid of broad beam analyses including quench crystals.

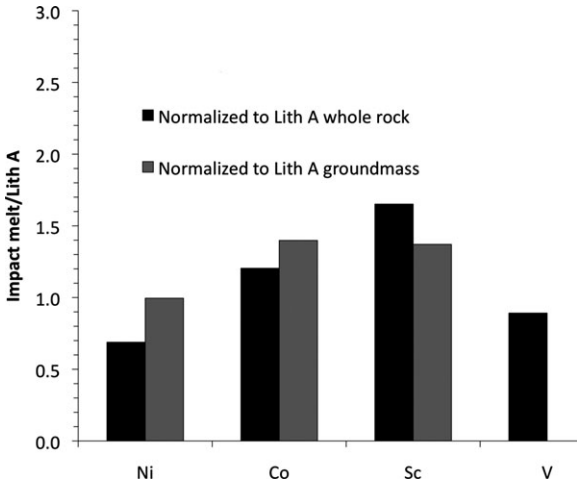

Fig. 4. Basaltic impact glass compositions of selected trace elements from this study normalized to Lith A whole rock (Mittlefehldt et al. 1999) and Lith A mesostasis (Warren et al. 1999). Both literature compositions are from INAA data.

fraction) component, while maskelynite, merrillite, and the sulfur species is added (positive fraction) to the Lith A composition.

For both models, we ran two cases. The unconstrained case provides the solution when sulfur is weighted according to the Lith C standard deviation, which is fairly large. Both unconstrained mixing models explain the major and minor element relationships equally well, but neither accurately reproduces the correct S abundance (Fig. 5a). In the constrained cases, we weighted S similarly to Si to force the models to fit S. Adding Ni to our models illustrates the weakness in models that rely only on major elements: both soil and sulfide incorporation models predict higher Ni than the

Table 4. Mixing models of Lith A bulk and minerals with Martian soil (Model 1) and Lith A sulfide (Model 2) to produce the observed Lith C composition in Table 3. The "unconstrained" cases weight the elemental fit based on the standard deviations in the Lith C composition; the "constrained" cases increase the weighting of S to force the model to fit S.

	Model 1: Soil				Model 2: Sulfide			
	unconst.	±	const.	±	unconst.	±	const.	±
Bulk Lith A	98.7	10.61	100.0	9.83	102.8	9.59	103.4	9.55
Lith A olivine	−3.60	7.30	−3.6	7.40	−4.42	7.82	−5.04	7.70
Lith A maskelynite	3.28	2.80	3.11	2.78	2.62	2.84	2.51	2.86
Lith A merrillite	0.19	1.83	0.20	1.86	0.14	1.97	0.08	2.00
Lith A sulfide	–	–	–	–	0.02	0.26	0.10	0.04
Gusev soil	2.89	4.16	1.72	0.69	–	–	–	–
Σ	101.5	13.94	101.4	12.8	101.1	12.85	101.0	12.75
$\chi 2/\nu$	3.33		3.42		3.86		3.99	

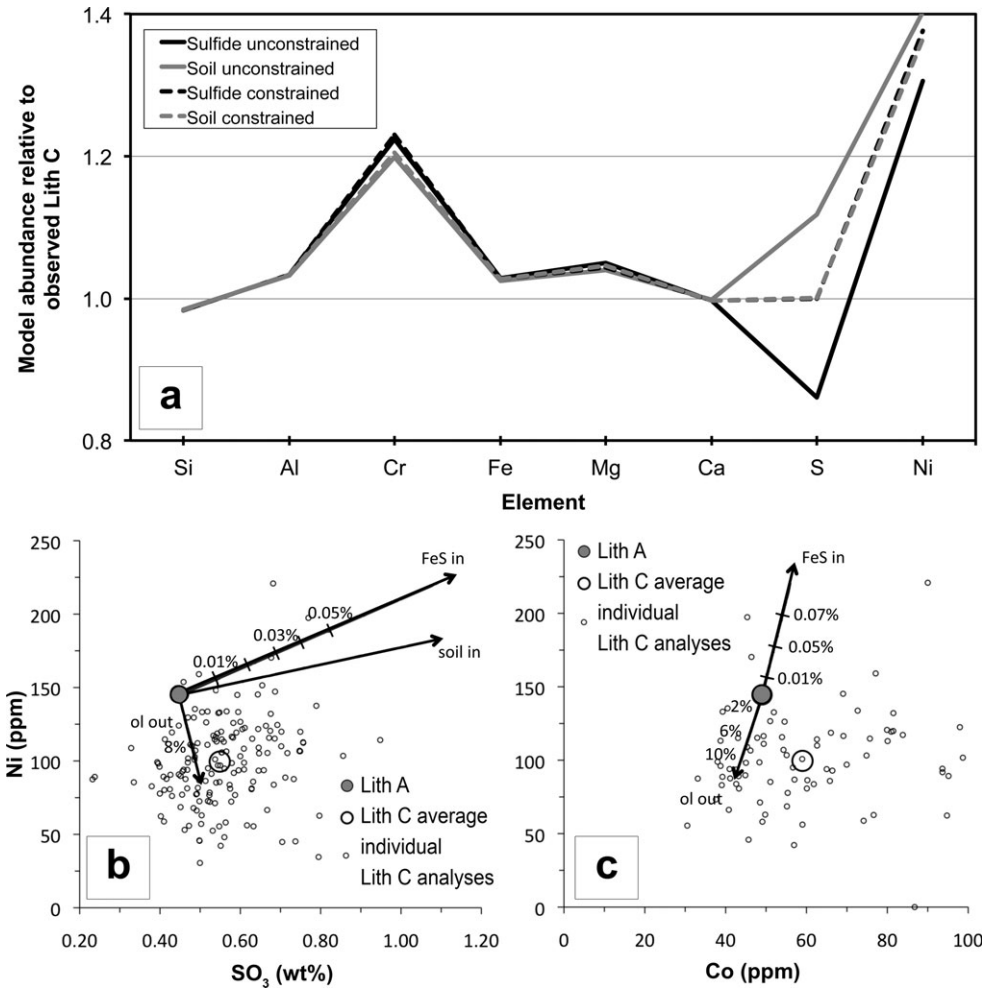

Fig. 5. Lith A melt composition with excess sulfide, added Martian soil, and residual olivine. a) Mixing model results relative to the observed Lith C composition. b) Ni-SO_3 diagram showing Lith A melt evolution with added excess sulfide (FeS) or added soil to Lith A. Modal percentages of added materials are indicated by the tick marks on the arrows. c) Ni-Co diagram showing Lith A melt evolution with added sulfide (FeS) and residual olivine. No Co data are available for Martian soil.

Lith C melt contains (100 ppm). If we had used a bright dust composition from Yen et al. (2005) and Yen et al. (2006), even less regolith could be accommodated and the Ni overabundance would be exacerbated as the bright dust contains more S and Ni than the MER-A average composition.

It is clear that the addition of regolith or sulfide or the subtraction of olivine alone cannot satisfactorily explain the Ni-S systematics of the shock melt. The addition of regolith or sulfide would drive the melt to Ni/S ratios higher than those measured unless coupled with >8% residual olivine (Fig. 5b)—considerably more than the 3% suggested by the model in Table 4. Also, no combination of these processes can explain the low Ni/Co compositions of the shock melt relative to Lith A (Fig. 5c). Incorporating the highest measured olivine Ni contents in the models for Table 4 and Fig. 5 does not appreciably change the results. Therefore, we look elsewhere for a source of these elements.

DISCUSSION

The Source of SO_3

We used elemental maps to examine the correlation of S-rich areas with other elements to determine its source (Fig. 6). Some pyrrhotite grains have coincident Fe and S signatures, but there are a number of locations where S does not obviously correlate with Fe, Mg, or Ca. One of these high-S signatures coincides with a relatively high-Al region, but the Al concentration is diffuse and no grains are visible. These domains are likely partly mixed Al-S phases such as the decrepitated grains observed by Gooding et al. (1988).

Quantitative element relations for all shock melt glass analyses show these correlations in more detail (Fig. 7). None of the elements are convincingly correlated with SO_3, although evaluation by a two-tailed T-test show that Al_2O_3-SO_3 and Ni-SO_3 are correlated and MgO-SO_3 (Fig. 7d) are anti-correlated at the 99% confidence level ($\alpha < 0.01$). Rao et al. (2003, 2004) also found positive Al_2O_3-SO_3 correlations in some Lith A shock melt glasses; however, unlike our work, they found a positive CaO-SO_3 correlation in some melt pockets. This could indicate that some shock melt pods contain a secondary Ca-S phase.

That FeO does not correlate with SO_3 suggests that Fe-sulfide (or Fe-sulfate) is not the carrier of S into the shock melt. This is further supported by the presence of some S-rich regions without correspondingly high Fe in Fig. 6. Likewise, in our analyses we see no CaO-SO_3 correlation, meaning that gypsum is not a likely secondary mineral bringing S into the melt.

The weakly positive Ni-SO_3 correlation shown in Fig. 7f might indicate a sulfide carrier of S into the melt but this is not supported by the FeO-SO_3 relationships since Ni is only observed in Fe-rich sulfides in EET 79001. Yen et al. (2006) suggested that Mg-sulfate might be a major carrier of Ni on the Martian surface and would thus be a potential regolith component or an alteration phase formed in situ in Lith A, but the MgO-SO_3 anti-correlation does not support this process here. Also, not shown in Fig. 7, Ni is not correlated significantly with any other oxide measured in the glass besides SO_3, including MgO ($r^2 = -0.04$).

The weakly positive Al_2O_3-SO_3 correlation might suggest the presence of S-bearing Al-silicates, identified by Gooding and Muenow (1986) in Lith A prior to melting, or Al-sulfates, which have been detected in the Martian regolith, possibly as products of acid-sulfate alteration (Morris et al. 2005; Wang et al. 2006; Hurowitz and McLennan 2007). Hurowitz et al. (2005) experimentally exposed a synthetic shergottite to acid-sulfate alteration conditions, producing alunogen ($Al_2(SO_4)_3 \cdot 17H_2O$), along with Fe- and Ca-sulfates, and high Na/Al in the effluent, demonstrating that the acid-sulfate effect on plagioclase and glass to be a stripping of alkalis and relative immobility of Al. We explored the implications of this source further by considering K as a tracer of Al_2O_3-bearing feldspar sources.

Figure 8 demonstrates that K systematics cannot be fully explained by the addition of feldspar or the subtraction of olivine, regardless of whether regolith or sulfide was added. The abundance of K_2O relative to Al_2O_3 should increase by these processes (Fig. 8a), when in fact it decreases in the shock melt, and Na/K relative to Al_2O_3 is higher than these models predict (Fig. 8b). Alkali loss to impact volatilization is unlikely because Na is expected to be as volatile as K, or more, during impact processes (McDonough and Sun 1995). This suggests K was lost relative to Na prior to impact.

The decoupling of K and Na can also be explained by relatively K-rich (low Na_2O/K_2O) phases in Lith A succumbing to leaching by S-rich, acidic fluids. Such a fluid would have worked its way along vugs and fractures, leaching K and depositing secondary minerals (McSween and Jarosewich 1983; Gooding and Muenow 1986; Gooding et al. 1988). In Gusev Crater, Haskin et al. (2005) reported at least three rocks investigated by MER-A (Humphrey, Adirondack, and Mazatzal) that showed secondary minerals filling vugs connected by veins—an analogous, although more advanced situation as we propose. The mesostasis phases, e.g., alkali-rich feldspar and devitrified late-stage glasses, in Lith A are the repository of much of the bulk K_2O, having Na_2O/K_2O <0.5 (Steele and Smith 1982), while bulk Lith A has Na_2O/K_2O of 16.8 (McSween and Jarosewich 1983). Because these K-rich phases are fine-grained and represent the lowest crystallization temperatures, they would be particularly vulnerable to alteration.

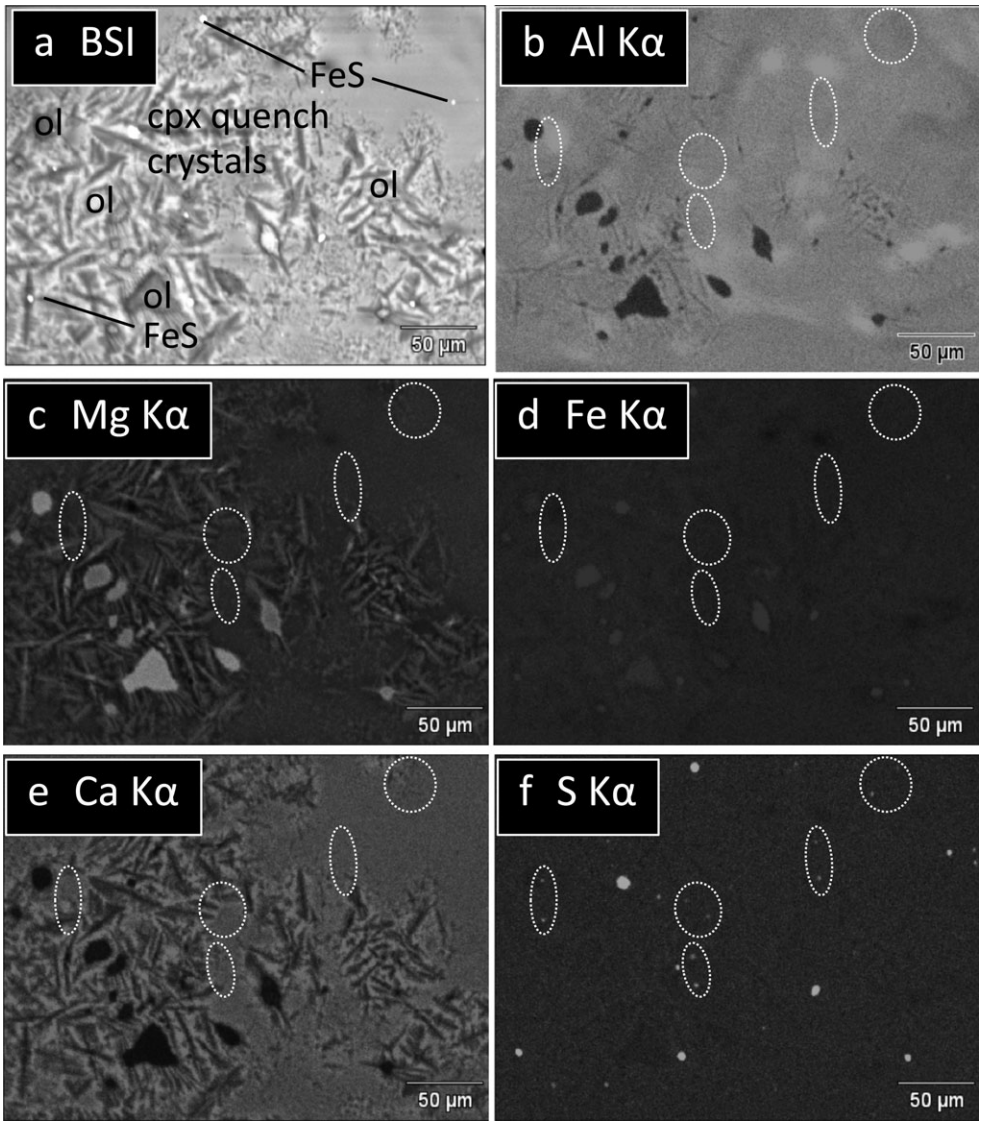

Fig. 6. BSI and X-ray elemental maps for a glass and quench crystal-rich portion of EET 79001,18. a) Backscattered-electron image with examples of olivine (ol), pyrrhotite (FeS), and quench crystals of clinopyroxene (cpx). A comparison of correlated bright spots on the Fe (d) and S (f) maps indicate the presence of pyrrhotite grains, but a number of S-rich spots are circled on the element maps (b–f) where S does not correlate to Fe. There are no apparent correlation between S and Ca. Although many of the S-rich spots coincide with Al-rich patches or schlieren there are no discrete Al-S grains visible.

Sulfur Speciation and fO_2 of the Shock Melt

In the previous section, we suggest that the source of S may be Al-sulfates observed by Gooding and Muenow (1986). However, Fig. 9 compares wavescans of the S K-alpha peaks in the shock melt glass to the peak locations in the standards for pyrrhotite (S^{2-}) and anhydrite (S^{6+}). The peak location in the glass matches the pyrrhotite standard, indicating that most of the S in the shock melt was reduced at the time of quenching. This supports the results of micro-Xanes in situ analysis by Sutton et al. (2008) and Walton et al. (2010), who found S in the shock melt glasses in both Lith A and Lith B to be dominantly reduced and occurring as sulfide, not sulfate.

Sutton et al. (2008) suggested that sulfide in the melt might be the product of sulfate reduction during impact shock. Conversely, Walton et al. (2010) and Walton (2013) used phase stability relationships to show that the shock pressure experienced by EET 79001 was relatively high (~18 GPa) for a short duration (0.01s). Based on the experiments of Wilke et al. (2008), Walton et al. (2010) suggested that the short duration of shock would be insufficient to reduce S^{6+} to S^{2-} in one of EET 79001's ~1 cm sized shock melt pockets.

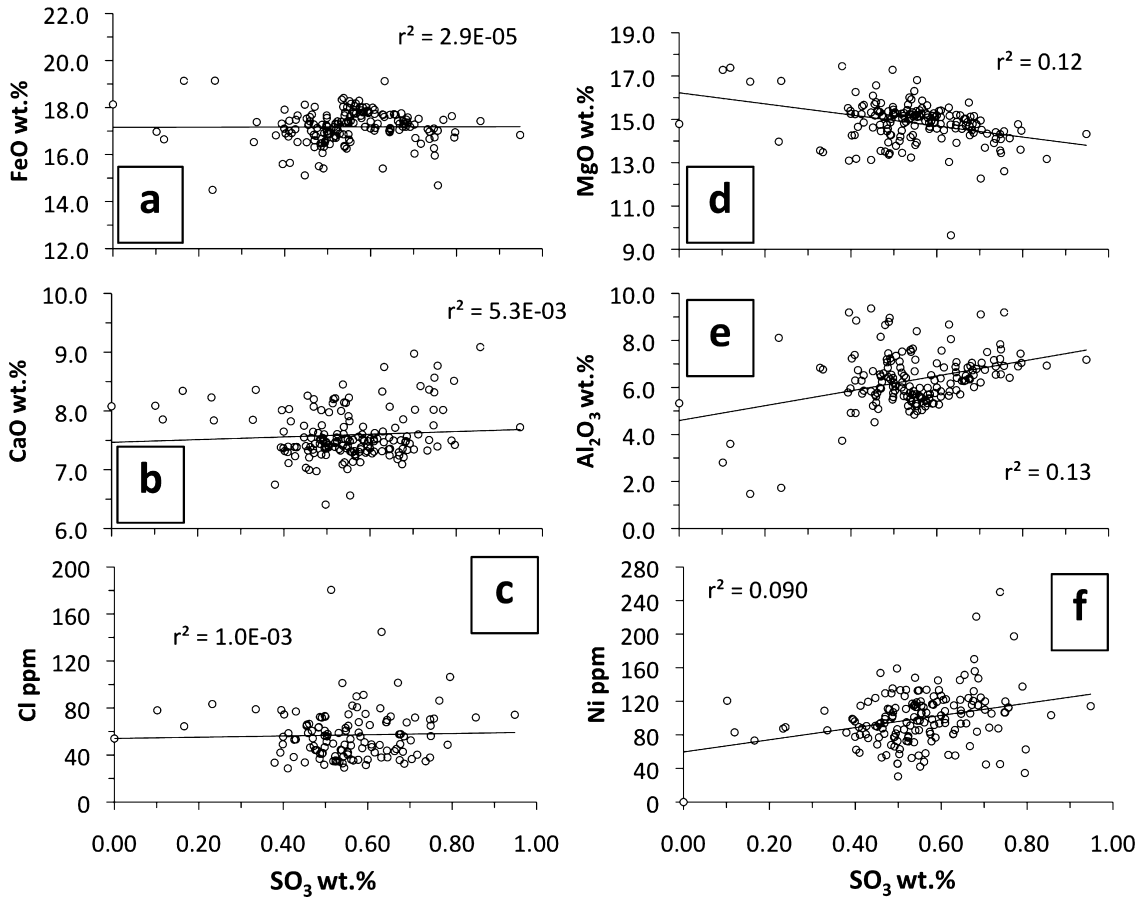

Fig. 7. Scatter plots showing variation in oxides and elements with SO_3: a) FeO, b) CaO, c) Cl, d) MgO, e) Al_2O_3, f) Ni. Each graph has a regression line, and an r^2 value. The relationships are discussed in the text.

However, we proffer that the Wilke et al. (2008) experiments are not a convincing analog for EET 79001 shock melting. They held a sulfate-bearing glass of synthetic andesite composition at 1.0 GPa and 1300 °C in a reducing graphite capsule and after 30 min found that the reduction front behind which sulfate converted to sulfide advanced <50 μm. First, conditions experienced by EET 79001 were likely ≥31 GPa (Fritz et al. 2005), an order of magnitude higher than Wilke et al.'s (2008) conditions, and there is no known means to scale their results to the conditions of planetary impact. Second, glassy impact-related materials, such as fulgurites and tektites, are reduced relative to their source materials by a process involving disequilibrium devolatilization inherent to the impact process that causes oxygen-loss and thus reduction in the melt (Melosh and Artemieva 2004; Sheffer and Melosh 2005; Sheffer et al. 2006). Wilke et al.'s (2008) experimental conditions would not follow the pressure-entropy path of an impact as discussed by Melosh and Artemieva (2004), would not lead to catastrophic devolatilization, and thus the experiments are probably not good matches for impact-reduction. Therefore, we reason that sulfate reduction to sulfide in the EET 79001 shock melt may have been an efficient and relatively comprehensive process, permitting the primary carrier of sulfur to be an Al-sulfate phase.

Chlorine, Cl/SO_3, and Martian Fluids

We further explore the possibility of the S carrier being a fluid-deposited sulfate by examining the fluid-mobile element Cl. Shergottites are generally Cl-poor (compared to nakhlites and surface rocks analyzed by MER) but have moderate SO_3 contents. This basic relationship is preserved in the EET 79001 shock melt.

The EET 79001 shock melt contains 57 ppm Cl on average with 124 of 164 analyses yielding Cl above the 27 ppm 2-sigma d.l. (Table 3) and an average of 43 ppm if all analyses b.d.l. are included in the average as zeros. We did not analyze Cl in Lith A minerals, and the only reported analysis for Cl in the bulk EET 79001 Lith A yielded 26 ppm (Burghele et al. 1983). While our Cl values in the shock melt are above detection limits,

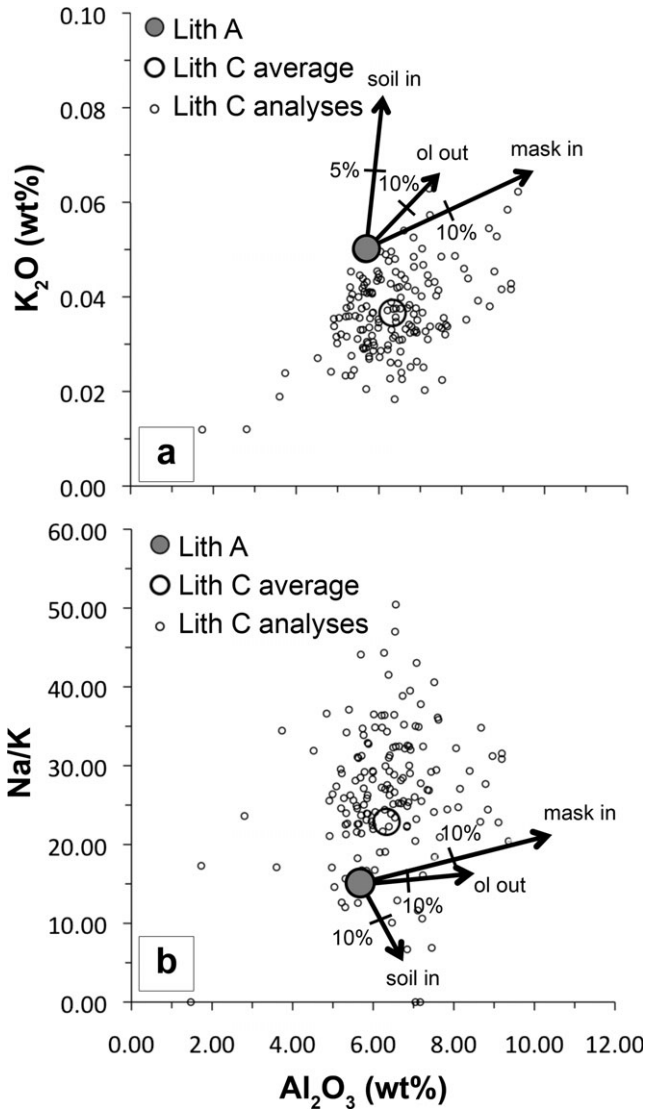

Fig. 8. K_2O-Al_2O_3 and Na/K-Al_2O_3 showing Lith A melt evolution with excess feldspar (maskelynite = mask), added Martian soil, or residual olivine. a) In K_2O-Al_2O_3 space, all of the melt pathways lead away from the measured Lith C shock melt (IM) compositions, particularly with regard to K_2O. b) In Na/K-Al_2O_3 space, none of the phase additions or subtractions lead through the field of measured data.

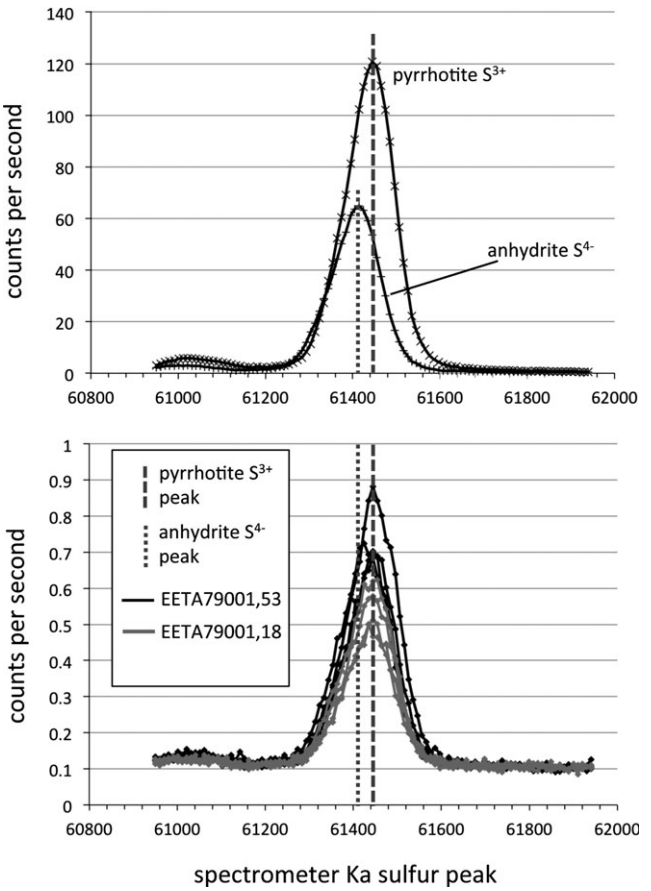

Fig. 9. Wavescans of the pyrrhotite (S^{2-}) and anhydrite (S^{6+}) standards and of the shock melt glass. The peak locations of the shock melt glasses match closely with the reduced sulfur in the pyrrhotite standard.

there is a possibility that some Cl comes from the thin section epoxy. Thus, we cannot say with surety that the EET 79001 shock melt is enriched in Cl relative to Lith A. Regardless, even considering possible epoxy contamination, we find a very low abundance of Cl compared to that found in secondary Martian minerals in nakhlites and low compared to shock melts in other shergottites (Stoffler et al. 1986; Gooding et al. 1990; Treiman et al. 1993; Dreibus et al. 1999; Rao et al. 2008).

We find the shock melt glass to be less enriched in SO_3 than Rao et al. (1999) or Walton et al. (2010) (Table 3), but the shock melt SO_3/Cl of >96 is still very high compared with Martian fluids (Schmidt et al. 2009). More rigorous attempts to constrain SO_3/Cl in EET 79001 Lith A are complicated by low Cl values near or below the detection limit (Gooding et al. 1990; Rao et al. 2008). Our range of 96–128 is lower than the bulk Lith A SO_3/Cl of ~170 based on McSween and Jarosewich's (1983) SO_3 data and the Burghele et al. (1983) Cl values. The fact remains that addition of regolith in the amounts needed to match the S data would have added much more Cl to the shock melt than is observed.

These data further support our hypothesis for S enrichment from alteration phases, although any fluid phase in contact with EET 79001 must have been S-rich and Cl-poor. Schmidt et al. (2009) and Rao et al. (2008, 2009) demonstrate that Martian surface rocks and meteorites have interacted with multiple, possibly temporally distinct, fluids of varying chemistries, and that most are either S-rich, Cl-poor or S-poor, Cl-rich endmembers. In agreement with Rao et al. (2008), we

interpret the high SO_3/Cl in EET 79001 as reflecting interaction with a fluid on Mars that was relatively S-rich and Cl-poor.

CONCLUSIONS

Our work shows that neither incorporation of Martian regolith nor excess melting of sulfide can be the sole, or perhaps even primary, agent of S enrichment in the EET 79001 shock melt. The amount of regolith or sulfide sufficient to deliver the excess S would result in much more Cl and Ni in the shock melt glass than is present. In fact, the glass is somewhat depleted in Ni relative to Lith A. The presence of residual olivine could explain some relative Ni depletion in the melt, but it cannot account for sufficient Ni depletion to permit the hypotheses of regolith or sulfide addition, nor do these mechanisms explain the high Co contents in the melt relative to Lith A. Likewise, the garnishing of Ni by sulfide phases entrained in Lith C is not sufficient to explain the deficit. Addition of Martian regolith to the shock melt would also contribute much more Cl than is observed. Furthermore, the lack of a significant correlation of S-rich areas in Lith C with Fe shows that melted pyrrhotite was not the primary carrier of S into the shock melt. The alteration processes that delivered S also leached some K and Ni out of the rock.

We offer the following hypothesis for the formation of Lith C in EET 79001, illustrated in Fig. 10. EET 79001 Lith A crystallized from a basaltic magma with mafic megacrysts at or near the Martian surface. The latest and lowest temperature stages of crystallization and quenching produced a mesostasis composed of relatively K-rich feldspar and glass, as observed by Steele and Smith (1982) (Fig. 10a). Coincident with or subsequent to the formation of the mesostasis, Lith A was infiltrated by small amounts of high S/Cl fluid that was likely externally derived (Fig. 10b). This fluid preferentially attacked the finest-grained material along fractures and vapor pathways, including the K-rich mesostasis, stripping some of the K from the material and depositing Al-sulfates in addition to other minerals. Such Al-sulfate phases are stable under water-limited, high-S fluid conditions (Hurowitz et al. 2005) and occur in EET 79001 in vugs, cracks, and as partially decrepitated grains entrained in the shock melt (Gooding et al. 1988). The most permeable regions of the Lith A basalt would not only experience the most fluid interaction, but would also serve as foci for shock-induced melting (McSween and Jarosewich 1983; Gooding and Muenow 1986; Gooding et al. 1988), as expected from modeling and observation of shock effects (Stöffler et al. 1991; Walton et al. 2007, 2010; Walton 2013) (Fig. 10c). The secondary minerals in these regions, having formed at the lowest temperatures and being the finest grained, would be the most susceptible to melting and incorporation into Lith C (Fig. 10d).

Incorporation of these Martian alteration/weathering products explains element correlations in Lith C, particularly the deficit of K relative to Na, and enriched S positively correlated with Al. The shock-melting process resulted in the reduction of the secondary sulfate to sulfide. A similar scenario was offered to explain the enriched F, S, and REEs in Tissint (Aoudjehane et al. 2012). Additionally, this scenario further supports the findings of Rao et al. (2008) that EET 79001 was subjected to a fluid of relatively high SO_3/Cl. Although the Martian surface is enriched in Cl as well as S, this provides further evidence that these elements have been decoupled in the Martian geologic past.

The observed Ni depletion in the shock melt is strong evidence against the incorporation of regolith or excess sulfide even while its cause is difficult to constrain. Nickel mobility under Martian surface conditions has been demonstrated by data from the Mars Exploration Rovers (Yen et al. 2006). There may have been partial leaching of olivine as well as mesostasis and feldspar during fluid alteration, which could partly explain the observed anti-correlation of Mg and S in Lith C. Olivine destruction proceeds quickly in basalts of Martian compositions under acid-sulfate conditions, and these fluids may transport olivine components out of the system (Tosca et al. 2004; Hurowitz and McLennan 2007).

However, it is clear that the EET 79001 shock melt pockets record interaction with the Martian atmosphere, both directly as trapped gases (Bogard and Johnson 1983), and indirectly in isotopic signatures. Rao et al. (2002, 2011) measured excess neutron-capture ^{80}Kr from Br, as well as a correlated decrease in Sm, in shock melt relative to the Martian atmosphere. They suggested that this signature was generated in situ in the regolith, which was then injected as melt into the meteorite during impact and ejection from the Martian surface. Samarium is present in Lith A in concentrations of ~0.78 ppm and bromine at ~60 ppm in Martian soils (Mittlefehldt et al. 1999; Warren et al. 1999; Yen et al. 2005)—both below EMP detection limits. If small changes to the concentrations of these elements were made by hydrothermal alteration or by mechanisms proposed by Rao et al. (2011), we would not be able to detect any mass change in Br, Sm or noble gases by our methods. The glass compositions we determined by EMP place an upper limit on the amounts of any known regolith composition that can be incorporated into either of the shock melt pods we

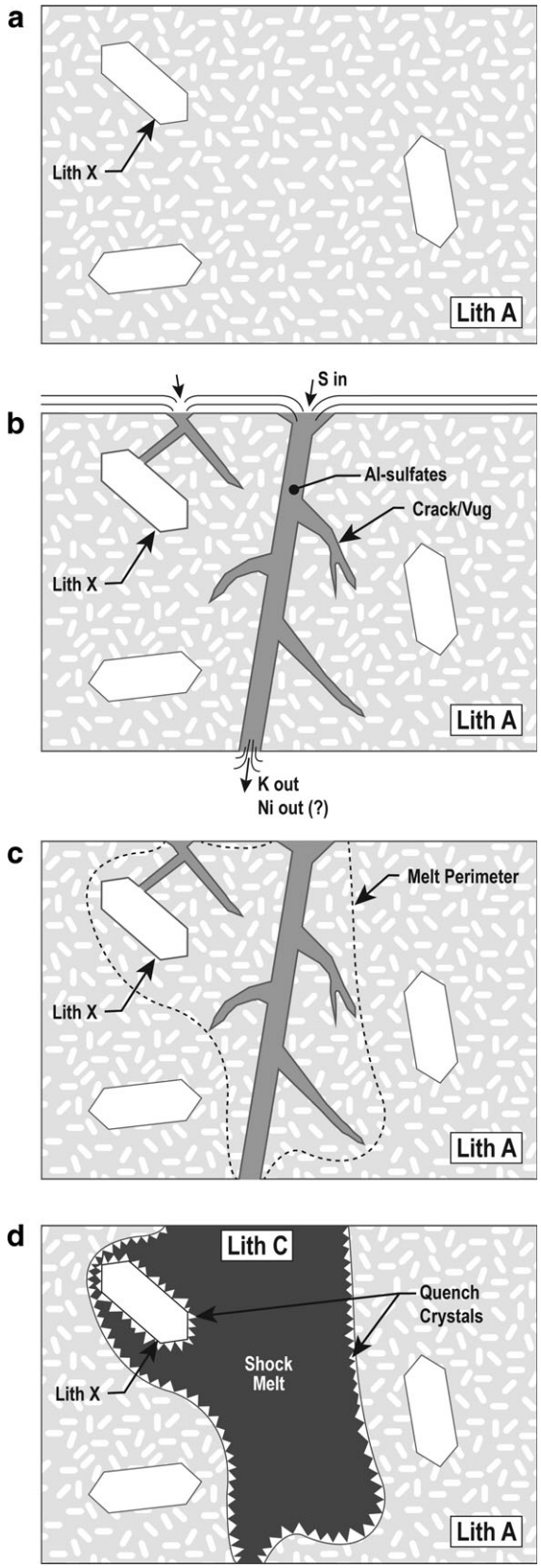

Fig. 10. Schematic diagram of our suggested scenario for the formation of the shock melt (Lith C). a) Lith A including Lith X (megacrystal olivine and pyroxene) prior shortly after cooling. b) Infiltration of high S/Cl fluids along cracks and pores introduces excess S, leaches some K and Ni, and deposits secondary minerals. c) Shock impedance contrasts between open spaces (vugs and cracks) and groundmass concentrate shock energy. d) Lith C is composed of shock melt, surviving megacrysts (now relict), and quench crystals nucleating on unmelted surfaces.

examined, but cannot rule out trace amounts of regolith entering or leaving the system.

Acknowledgments—We thank the NASA Postdoctoral Program for funding salary and travel for the first author, and the Antarctic Meteorite Working Group for approving our sample request. Joel Hurowitz, Hap McSween, Paul Warren, Erin Walton, and several anonymous reviewers provided helpful reviews and editor Mike Zolensky encouraged us through several revisions. This research was supported by a Mars Fundamental Research Program grant to B. A. Cohen and used NASA's Astrophysics Data System (ADS).

Editorial Handling—Dr. Michael Zolensky

REFERENCES

Aoudjehane H. C., Avice G., Barrat J.-A., Boudouma O., Chen G., Duke M. J. M., Franchi I. A., Gattacceca J., Grady M. M., Greenwood R. C., Herd C. D. K., Hewins R., Jambon A., Marty B., Rochette P., Smith C. L., Sautter V., Verchovsky A., Weber P., and Zanda B. 2012. Tissint Martian meteorite: A fresh look at the interior, surface, and atmosphere of Mars. *Science* 338:785–788.

Armstrong J. T. 1988. Quantitative analysis of silicate and oxide materials: comparison of Monte Carlo, ZAF, and ϕ (ρ Z) procedures. In *Microbeam analysis*, edited by Newbury D. E. San Francisco: San Francisco Press. pp. 239–246.

Barrat J. A., Jambon A., Ferrière L., Bollinger C., Langlade J. A., Liorzou C., Boudouma O., and Fialin M. 2014. No Martian soil component in shergottite meteorites. *Geochimica et Cosmochimica Acta* 125:23–33.

Bishop J. L., Murchie S. L., Pieters C. M., and Zent A. P. 2002. A model for formation of dust, soil, and rock coatings on Mars: Physical and chemical processes on the Martian surface. *Journal of Geophysical Research* 107: doi:10.1029/2001JE001581.

Blake D. F., Morris R. V., Kocurek G., Morrison S. M., Downs R. T., Bish D., Ming D. W., Edgett K. S., Rubin D., Goetz W., Madsen M. B., Sullivan R., Gellert R., Campbell I., Treiman A. H., McLennan S. M., Yen A. S., Grotzinger J., Vaniman D. T., Chipera S. J., Achilles C. N., Rampe E. B., Sumner D., Meslin P.-Y., Maurice S., Forni O., Gasnault O., Fisk M., Schmidt M., Mahaffy P., Leshin L. A., Glavin D., Steele A., Freissinet C., Navarro-González R., Yingst R. A., Kah L. C., Bridges

N., Lewis K. W., Bristow T. F., Farmer J. D., Crisp J. A., Stolper E. M., Des Marais D. J., and Sarrazin P. 2013. Curiosity at Gale Crater, Mars: Characterization and analysis of the Rocknest Sand Shadow. *Science* 341:5.

Bogard D. D. and Johnson P. 1983. Martian gases in an Antarctic meteorite? *Science* 221:651–654.

Burghele A., Dreibus G., Palme H., Rammensee W., Spettel B., Weckwerth G., and Wanke H. 1983. Chemistry of shergottites and the shergotty parent body (spb): Further evidence for the two component model of planet formation. Proceedings, 14th Lunar and Planetary Science Conference. pp. 80–81.

Donovan J. J. 2014. Reports and notes on electron microprobe analysis at the University of Oregon. http://epmalab.uoregon.edu/reports.htm.

Donovan J. J., Snyder D. A., and Rivers M. L. 1993. An improved interference correction for trace element analysis. *Microbeam Analysis* 2:23–28.

Dreibus G., Spettel B., Huth J., and Zipfel J. 1999. Halogens in Nakhla: Terrestrial or Martian origin? *Meteoritics and Planetary Science Supplement* 34:33.

Fritz J., Artemieva N., and Greshake A. 2005. Ejection of Martian meteorites. *Meteoritics and Planetary Science* 40:1393–1411.

Gellert R., Rieder R., Anderson R. C., Brückner J., Clark B. C., Dreibus G., Economou T., Klingelhöfer G., Lugmair G. W., Ming D. W., Squyres S. W., d'Uston C., Wänke H., Yen A., and Zipfel J. 2004. Chemistry of rocks and soils in Gusev Crater from the alpha particle X-ray spectrometer. *Science* 305:829–833.

Gellert R., Rieder R., Brückner J., Clark B. C., Dreibus G., Klingelhöfer G., Lugmair G., Ming D. W., Wänke H., Yen A., Zipfel J., and Squyres S. W. 2006. Alpha particle x-ray spectrometer (APXS): Results from Gusev crater and calibration report. *Journal of Geophysical Research (Planets)* 111: doi:10.1029/2005JE002555.

Gooding J. L. and Muenow D. W. 1986. Martian volatiles in shergottite EETA79001—New evidence from oxidized sulfur and sulfur-rich aluminosilicates. *Geochimica et Cosmochimica Acta* 50:1049–1059.

Gooding J. L., Wentworth S. J., and Zolensky M. E. 1988. Calcium carbonate and sulfate of possible extraterrestrial origin in the EETA79001 meteorite. *Geochimica et Cosmochimica Acta* 52:909–915.

Gooding J. L., Aggrey K. E., and Muenow D. W. 1990. Volatile compounds in shergottite and nakhlite meteorites. *Meteoritics* 25:281–289.

Goodrich C. A. 2002. Olivine-phyric Martian basalts: A new type of shergottite. *Meteoritics and Planetary Science* 37:31.

Haskin L. A., Wang A., Jolliff B. L., McSween H. Y., Clark B. C., Des Marais D. J., McLennan S. M., Tosca N. J., Hurowitz J. A., Farmer J. D., Yen A., Squyres S. W., Arvidson R. E., Klingelhöfer G., Schröder C., de Souza P. A., Ming D. W., Gellert R., Zipfel J., Brückner J., Bell J. F., Herkenhoff K., Christensen P. R., Ruff S., Blaney D., Gorevan S., Cabrol N. A., Crumpler L., Grant J., and Soderblom L. 2005. Water alteration of rocks and soils on Mars at the Spirit rover site in Gusev Crater. *Nature* 436:66–69.

Herd C. D. K., Dwarzski R. E., and Shearer C. K. 2009. The behavior of Co and Ni in olivine in planetary basalts: An experimental investigation. *American Mineralogist* 94:244–255.

Humayun M., Nemchin A., Zanda B., Hewins R. H., Grange M., Kennedy A., Lorand J. P., Gopel C., Fieni C., Pont S., and Deldicque D. 2013. Origin and age of the earliest Martian crust from meteorite NWA 7533. *Nature* 503:513–516.

Hurowitz J. A. and McLennan S. M. 2007. A ~3.5 Ga record of water-limited, acidic weathering conditions on Mars. *Earth and Planetary Science Letters* 260:432–443.

Hurowitz J. A., McLennan S. M., Lindsley D. H., and Schoonen M. A. A. 2005. Experimental epithermal alteration of synthetic Los Angeles meteorite: Implications for the origin of Martian soils and identification of hydrothermal sites on Mars. *Journal of Geophysical Research (Planets)* 110:7002.

Korotev R. L., Haskin L. A., and Jolliff B. L. 1995. A simulated geochemical rover mission to the Taurus-Littrow valley of the Moon. *Journal of Geophysical Research* 100:14,403–14,420.

Lorand J.-P., Chevrier V., and Sautter V. 2005. Sulfide mineralogy and redox conditions in some shergottites. *Meteoritics and Planetary Science* 40:1257–1272.

McDonough W. F. and Sun S.-S. 1995. The composition of the Earth. *Chemical Geology* 120:223–253.

McSween H. Y. and Jarosewich E. 1983. Petrogenesis of the Elephant Moraine A79001 meteorite: Multiple magma pulses on the shergottite parent body. *Geochimica et Cosmochimica Acta* 47:1501–1513.

McSween H. Y., Ruff S. W., Morris R. V., Gellert R., Klingelhöfer G., Christensen P. R., McCoy T. J., Ghosh A., Moersch J. M., Cohen B. A., Rogers A. D., Schröder C., Squyres S. W., Crisp J., and Yen A. 2008. Mineralogy of volcanic rocks in Gusev crater, Mars: Reconciling Mössbauer, alpha particle X-ray spectrometer, and miniature thermal emission spectrometer spectra. *Journal of Geophysical Research (Planets)* 113:E06S04.

Melosh H. J. and Artemieva N. 2004. How does tektite glass lose its water? (abstract #1723). 35th Lunar and Planetary Science Conference. CD-ROM.

Mittlefehldt D. W., Lindstrom D. J., Lindstrom M. M., and Martinez R. R. 1999. An impact melt origin for Lithology A of Martian meteorite EETA79001. *Meteoritics and Planetary Science* 34:357–367.

Morris R. V., Ming D. W., Graff T. G., Arvidson R. E., Bell J. F., Squyres S. W., Mertzman S. A., Gruener J. E., Golden D. C., Le L., and Robinson G. A. 2005. Hematite spherules in basaltic tephra altered under aqueous, acid-sulfate conditions on Mauna Kea volcano, Hawaii: Possible clues for the occurrence of hematite-rich spherules in the Burns formation at Meridiani Planum, Mars. *Earth and Planetary Science Letters* 240:168–178.

Newsom H. E. and Hagerty J. J. 1997. Chemical components of the Martian soil: Melt degassing, hydrothermal alteration, and chondritic debris. *Journal of Geophysical Research* 102:19,345–19,356.

Newsom H. E., Hagerty J. J., and Goff F. 1999. Mixed hydrothermal fluids and the origin of the Martian soil. *Journal of Geophysical Research* 104:8717–8728.

Rao M. N., Borg L. E., McKay D. S., and Wentworth S. J. 1999. Martian soil component in impact glasses in a Martian meteorite. *Geophysical Research Letters* 26:3265–3268.

Rao M. N., Bogard D. D., Nyquist L. E., McKay D. S., and Masarik J. 2002. Neutron capture isotopes in the Martian

regolith and implications for Martian atmospheric noble gases. *Icarus* 156:352–372.
Rao M. N., McKay D. S., and Stansbery E. 2003. Characterization of Martian soil fines fraction in SNC meteorites (abstract #1252). 34th Lunar and Planetary Science Conference. CD-ROM.
Rao M. N., Wentworth S. J., McKay D. S., and Stansbery E. 2004. Chemical weathering records of Martian soils preserved in the Martian Meteorite EET 79001 (abstract #1501). 35th Lunar and Planetary Science Conference. CD-ROM.
Rao M. N., Nyquist L. E., Wentworth S. J., Sutton S. R., and Garrison D. H. 2008. The nature of Martian fluids based on mobile element studies in salt-assemblages from Martian meteorites. *Journal of Geophysical Research (Planets)* 113:6002.
Rao M. N., Nyquist L. E., Sutton S. R., Dreibus G., Garrison D. H., and Herrin J. 2009. Fluid-evaporation records preserved in salt assemblages in Meridiani rocks. *Earth and Planetary Science Letters* 286:396–403.
Rao M. N., Nyquist L. E., Bogard D. D., Garrison D. H., Sutton S. R., Michel R., Reedy R. C., and Leya I. 2011. Isotopic evidence for a Martian regolith component in shergottite meteorites. *Journal of Geophysical Research* 116:08006.
Reed S. J. B. 2005. *Electron microprobe analysis and scanning electron microscopy in geology*. Cambridge: Cambridge University Press.
Rieder R., Gellert R., Anderson R. C., Brückner J., Clark B. C., Dreibus G., Economou T., Klingelhöfer G., Lugmair G. W., Ming D. W., Squyres S. W., d'Uston C., Wänke H., Yen A., and Zipfel J. 2004. Chemistry of rocks and soils at Meridiani Planum from the alpha particle X-ray spectrometer. *Science* 306:1746–1749.
Schmidt M. E., Farrand W. H., Johnson J. R., Schröder C., Hurowitz J. A., McCoy T. J., Ruff S. W., Arvidson R. E., Des Marais D. J., Lewis K. W., Ming D. W., Squyres S. W., and de Souza P. A. 2009. Spectral, mineralogical, and geochemical variations across Home Plate, Gusev Crater, Mars indicate high and low temperature alteration. *Earth and Planetary Science Letters* 281:258–266.
Sheffer A. and Melosh H. J. 2005. Why moldavites are reduced (abstract #1468). 36th Lunar and Planetary Science Conference. CD-ROM.
Sheffer A. A., Dyar M. D., and Sklute E. C. 2006. Lightning strike glasses as an analog for impact glasses: 57Fe Mössbauer spectroscopy of fulgurites (abstract #2009). Lunar and Planetary Science Conference. CD-ROM.
Smith M. R., Laul J. C., Ma M. S., Huston T., Verkouteren R. M., Lipschutz M. E., and Schmitt R. A. 1984. Petrogenesis of the SNC (shergottites, nakhlites, chassignites) meteorites: Implications for their origin from a large dynamic planet, possibly Mars. *Journal of Geophysical Research* 89:612.
Steele I. M. and Smith J. V. 1982. Petrography and mineralogy of two basalts and olivine-pyroxene-spinel fragments in achondrite EETA79001. *Journal of Geophysical Research: Solid Earth* 87:A375–A384.
Stoffler D., Ostertag R., Jammes C., Pfannschmidt G., Sen Gupta P. R., Simon S. B., Papike J. J., and Beauchamp R. H. 1986. Shock metamorphism and petrography of the Shergotty achondrite. *Geochimica et Cosmochimica Acta* 50:889–903.
Stöffler D., Keil K., and Scott E. R. D. 1991. Shock metamorphism of ordinary chondrites. *Geochimica et Cosmochimica Acta* 55:3845–3867.
Sutton S. R., Rao M. N., and Nyquist L. E. 2008. Sulfur and iron speciation in gas-rich impact-melt glasses from basaltic shergottites determined by MicroXANES (abstract #1961). 39th Lunar and Planetary Science Conference. CD-ROM.
Tosca N. J., McLennan S. M., Lindsley D. H., and Schoonen M. A. A. 2004. Acid-sulfate weathering of synthetic Martian basalt: The acid fog model revisited. *Journal of Geophysical Research* 109. doi:10.1029/2003JE002218.
Treiman A. H. 1995. S not equal to NC: Multiple source areas for Martian meteorites. *Journal of Geophysical Research* 100:5329–5340.
Treiman A. H., Barrett R. A., and Gooding J. L. 1993. Preterrestrial aqueous alteration of the Lafayette (SNC) meteorite. *Meteoritics* 28:86–97.
Wallace P. J. and Carmichael I. S. E. 1994. S speciation in submarine basaltic glasses as determined by measurements of S K-alpha X-ray wavelength shifts. *American Mineralogist* 79:161–167.
Walton E. L. 2013. Shock metamorphism of Elephant Moraine A79001: Implications for olivine–ringwoodite transformation and the complex thermal history of heavily shocked Martian meteorites. *Geochimica et Cosmochimica Acta* 107:299–315.
Walton E. L., Kelley S. P., and Spray J. G. 2007. Shock implantation of Martian atmospheric argon in four basaltic shergottites: A laser probe $^{40}Ar/^{39}Ar$ investigation. *Geochimica et Cosmochimica Acta* 71:497–520.
Walton E. L., Jugo P. J., Herd C. D. K., and Wilke M. 2010. Martian regolith in Elephant Moraine 79001 shock melts? Evidence from major element composition and sulfur speciation. *Geochimica et Cosmochimica Acta* 74:4829–4843.
Wang A., Haskin L. A., Squyres S. W., Jolliff B. L., Crumpler L., Gellert R., Schröder C., Herkenhoff K., Hurowitz J., Tosca N. J., Farrand W. H., Anderson R., and Knudson A. T. 2006. Sulfate deposition in subsurface regolith in Gusev crater, Mars. *Journal of Geophysical Research (Planets)* 111. doi:10.1029/2005JE002513.
Warren P. H., Kallemeyn G. W., and Kyte F. T. 1999. Origin of planetary cores: Evidence from highly siderophile elements in Martian meteorites. *Geochimica et Cosmochimica Acta* 63:2105–2122.
Wilke M., Jugo P. J., Klimm K., Susini J., Botcharnikov R., Kohn S. C., and Janousch M. 2008. The origin of S4+ detected in silicate glasses by XANES. *American Mineralogist* 93:235–240.
Yen A. S., Gellert R., Schröder C., Morris R. V., Bell J. F., Knudson A. T., Clark B. C., Ming D. W., Crisp J. A., Arvidson R. E., Blaney D., Brückner J., Christensen P. R., Desmarais D. J., de Souza P. A., Economou T. E., Ghosh A., Hahn B. C., Herkenhoff K. E., Haskin L. A., Hurowitz J. A., Joliff B. L., Johnson J. R., Klingelhöfer G., Madsen M. B., McLennan S. M., McSween H. Y., Richter L., Rieder R., Rodionov D., Soderblom L., Squyres S. W., Tosca N. J., Wang A., Wyatt M., and Zipfel J. 2005. An integrated view of the chemistry and mineralogy of Martian soils. *Nature* 436:49–54.
Yen A. S., Mittlefehldt D. W., McLennan S. M., Gellert R., Bell J. F., McSween H. Y., Ming D. W., McCoy T. J.,

Morris R. V., Golombek M., Economou T., Madsen M. B., Wdowiak T., Clark B. C., Jolliff B. L., Schröder C., Brückner J., Zipfel J., and Squyres S. W. 2006. Nickel on Mars: Constraints on meteoritic material at the surface. *Journal of Geophysical Research (Planets)* 111. doi:10.1029/2006JE002797.

SUPPORTING INFORMATION

Additional supporting information may be found in the online version of this article:

Appendix S1. All electron microprobe analyses of the shock melt lithology analyzed for this paper.